International Journal of Robotics and Control Systems
Vol. 6, No. 2, 2026, pp. 1405-1425
ISSN 2775-2658
http://pubs2.ascee.org/index.php/ijrcs

Robust LQR Control Design for High Efficiency Battery Supercapacitor Hybrid Storage Systems

Aissa Assas [a,1,*], Hocine Guentri [b,2], Tayeb Alaoui [c,3], Vojtech Blazek [d,4], Abdeldjalil Dahbi [e,5], Alfian Ma'arif [f,6], Ezzeddine Touti [g,7,*], Mohamed Metwally Mahmoud [h, i, 8,*]

[a] Department of Electrical Engineering, Institute of Technology, Energy Engineering and Computer Engineering Laboratory (L2GEGI), University Center Nour Bachir El Bayadh, El Bayadh 32000, Algeria
[b] Department of Electrical Engineering, Institute of Technology, Laboratory of Electronic Systems, Telecommunications and Renewable Energies (LESTRE), University Center Nour Bachir El Bayadh, El Bayadh 32000, Algeria
[c] Department of Electrical Engineering, Institute of Technology, Energy Engineering and Computer Engineering Laboratory (L2GEGI), University of Tiaret, Tiaret 14000, Algeria
[d] ENET Centre, CEET, VSB—Technical University of Ostrava, Ostrava 70800, Czech Republic
[e] Centre de Développement des Energies renouvelables (CDER), Unité de Recherche en Energies Renouvelables en Milieu Saharien (URERMS), Adrar 01000, Algeria
[f] Department of Electrical Engineering, Universitas Ahmad Dahlan, Yogyakarta 55191, Indonesia
[g] Center for Scientific Research and Entrepreneurship, Northern Border University, Arar 73213, Saudi Arabia
[h] Department of Electrical Engineering, Faculty of Energy Engineering, Aswan University, Aswan 81528, Egypt
[i] Jadara University Research Center, Jadara University, P.O Box 733, Irbid, Jordan
[1] a.assas@cu-elbayadh.dz; [2] hguentri2005@yahoo.fr; [3] tayeb.allaoui@univ-tiaret.dz; [4] vojtech.blazek@vsb.cz;
[5] dahbi_j@yahoo.fr; [6] alfian.maarif@te.uad.ac.id; [7] esseddine.touti@nbu.edu.sa; [8] metwally_m@aswu.edu.eg
* Corresponding Author

ARTICLE INFO

Article history
Received July 28, 2025
Revised April 17, 2026
Accepted May 01, 2026

Keywords
Photovoltaic;
Hybrid Energy Storage System;
Linear Quadratic Control;
Energy Management Optimization;
Power Fluctuation Attenuation

ABSTRACT

The integration of renewable energy sources into microgrid systems presents significant control challenges due to their inherent intermittency and rapid fluctuations in power output. This work proposes a robust control framework based on the LQR for managing a HESS composed of batteries and supercapacitors within a PV microgrid. Compared to conventional pole-placement techniques for tuning state-feedback regulators, the LQR approach offers notable advantages: it systematically optimizes control performance by balancing state regulation and control effort through adjustable weighting matrices; it ensures a globally optimal solution that enhances system stability and robustness under parameter uncertainties; and it simplifies the controller design process by avoiding complex pole assignment procedures, thus providing better scalability and ease of implementation. Through extensive simulation scenarios, the LQR-based controller demonstrates superior dynamic responses, including faster stabilization, reduced power fluctuation, and improved energy management efficiency. These results confirm that the LQR method significantly outperforms pole-placement strategies, offering a more reliable and adaptable control solution for advanced microgrid energy management in renewable-dominant environments.

1. Introduction

Over the past few decades, there has been a substantial increase in the integration of RESs for global electricity generation. In 2020, global PV solar electricity production reached 709.67 TWh, a 21.5% increase over 2019, accounting for 3.15% of global electricity production. In parallel, global WP generation totaled 698.043 TWh, reflecting a 17.65% year-over-year increase, and representing 4.8% of the world's electricity output [1]–[3]. This growth is driven by technological advancements and a commitment from governments and the public to accelerate the transition toward RESs [4]–[8].

However, due to the intermittent nature of RESs [9], [10], ESS plays a vital role in enhancing grid flexibility, reliability, and energy efficiency. In many microgrids, ESSs are essential to maintain energy balance and improve PQ [11]–[13]. Among storage technologies, batteries are widely utilized due to their high efficiency, but they pose several challenges. Batteries typically suffer from limited power density, which complicates their ability to meet peak power demands. Moreover, they introduce thermal management issues, capacity degradation under high-rate cycling, and shortened service life due to frequent charge–discharge cycles [14]–[16].

To mitigate these limitations, HESS has been proposed as a viable alternative [17], [18]. HESS offers several advantages, particularly in stand-alone renewable systems, including improved overall system efficiency, reduced operational costs, and extended ESS lifespan [19], [20]. Typically, a HESS integrates two complementary storage devices: one with high energy density and another with high power density [21], [22], most commonly a battery paired with a supercapacitor [23]–[25]. A primary challenge in HESS design lies in controlling and managing the battery/supercapacitor pair. Existing control methods are often divided into classical approaches, such as rule-based control [26], [27] and filter-based control [28], [29], and intelligent approaches, including artificial neural network-based control [30], [31], heuristic-based control [32], and FLC [33], [34].

Recent advances in control strategies for HESS have led to a variety of innovative approaches for optimizing the integration of batteries and supercapacitors, particularly in PV and microgrid applications. For example, Ref. [35] proposed a hybrid control method that combines FLC and SMC to regulate power converters in HESS, thereby improving robustness against disturbances and system nonlinearities. In a similar context, Ref. [36] developed an efficient energy management architecture for a grid-connected PV system with battery-supercapacitor storage. Their approach manages different operational modes through a multi-level control strategy, enhancing overall energy efficiency and reliability.

Ref. [37] introduced a genetic algorithm-based economic dispatch strategy for hybrid storage MGs, aiming to optimize system performance by minimizing operational costs while maintaining energy balance. Meanwhile, Ref. [38] presented a novel RB-EMS, complemented by a current estimation mechanism, for battery-supercapacitor HESS in a DC-MG architecture interfaced with the AC grid. This hybrid EMS strategy offers improved real-time power allocation and enhances dynamic performance. Ref. [39] extended this line of work by proposing a D-MPC framework for a HESS comprising SMES and batteries. Their method improves predictive accuracy and grid stability under varying generation conditions.

Additionally, several studies have focused on the combined control of batteries and supercapacitors using various methodologies. For instance, [39], [40] describes a hierarchical control system integrating batteries and supercapacitors for grid applications, featuring individual inner-loop current controllers for each storage branch and an outer-loop power-voltage controller to coordinate energy exchange and maintain voltage stability. Similarly, [41] proposed a unified control scheme for a standalone PV-based low-voltage DC-MG that manages both energy flow and DC bus voltage. However, the method is noted for its complexity in synthesis. Ref. [42] provided a comprehensive review of application scenarios for battery-supercapacitor HESS in MGs, highlighting the benefits of hybridization in improving PQ and energy resilience. Ref. [43] focused on the modeling of a bidirectional buck-boost converter in EVs for V2G applications. This setup diverts high-frequency power fluctuations to the supercapacitor, thereby prolonging battery life and stabilizing current flow.

Furthermore, Ref. [44] investigated control strategies for a standalone DC-MG comprising PV, battery, and supercapacitor elements, providing various approaches for coordinating power delivery and maintaining SOC balance. In another study, Ref. [45] examined heuristics-based power management in PV systems with hybrid battery-supercapacitor storage, showing promising results for real-time control under uncertain conditions. Ref. [46] also contributed a variable structure-based control technique for a fuel cell–battery–supercapacitor hybrid electric vehicle system, which dynamically adjusts control actions based on system states to enhance performance during transient operation.

In this paper, we propose a robust control framework based on the LQR, specifically designed for managing a HESS in a stand-alone PV system. We aim to enrich this growing research area by applying a robust and efficient method to improve HESS control and management. The paper's structure is as follows: Section 2 describes the DC grid configuration. Section 3 outlines the proposed method and presents the LQR-based control analysis of the HESS. Section 4 discusses the simulation results. Finally, Section 5 offers conclusions and perspectives.

2. DC Grid Configuration

The standalone system consists of PV panels supported by a HESS. The latter is a composition of batteries and supercondensers. Using an MPPT algorithm, a boost converter extracts the maximum power from the PV panels. Also, the converter is used to connect these panels to the DC bus. Each element of the hybrid storage system is connected to the DC bus using a buck-boost converter to provide power exchange with this DC bus, as shown in Fig. 1.

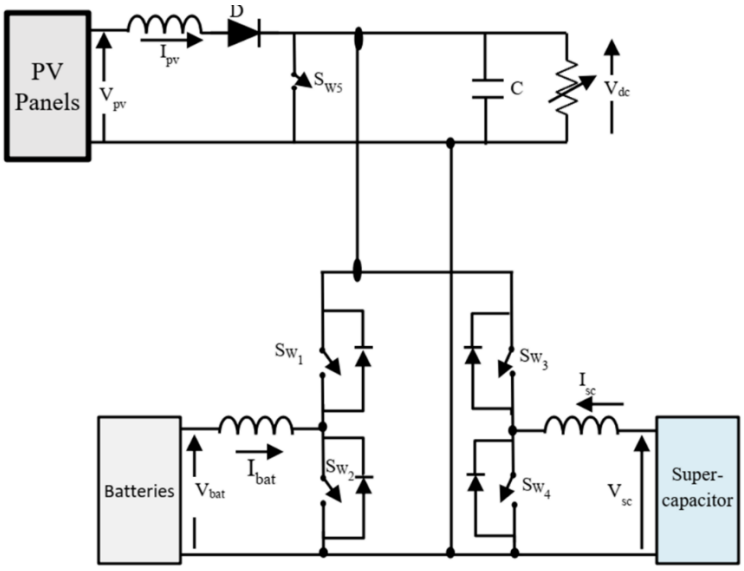

Fig. 1. Addressed system

Due to a mismatch between solar panel generation and variable load demand, the DC bus voltage was maintained at a constant level. When the PV panels' generation exceeds the demand, the DC bus voltage increases compared to its reference value. Therefore, the HESS will charge to absorb the excess power. Similarly, when the PV panels' generation is lower than the demand, the DC bus voltage decreases from its reference value. Consequently, the HESS system discharges to supply the power deficit. The variables I_{pv}, I_b, and I_{sc} represent the PV panel, battery, and SC currents, respectively. Additionally, V_{pv}, V_b, and V_{sc} represent the PV panels, batteries, and SC voltages, respectively. And L_{pv}, L_b, and L_{sc} represent the filter inductances of the boost converter, battery, and SC converters, respectively. V_{DC} is the DC bus voltage, C is the filter capacitance, and R is the load resistance. S_{w1}, S_{w2}, S_{w3}, S_{w4}, and S_{w5} are control switches as shown in Fig. 1.

3. Control Scheme of the Investigated System

3.1. Overview of the LQR

The goal of an LQR approach is to minimize the following quadratic performance index (J): [41], [42].

$$J = \int_0^{\infty} \left(x^T(t)Qx(t) + u^T(t)Ru(t)\right)dt \tag{1}$$

or in discrete form:

$$J = \sum_0^N \left(x^T(k).Q.x(k) + u^T(k).Q.u(k)\right) \tag{2}$$

where Q and R are positively defined weighting matrices.

The challenge is to find a control law $u(k)$ that minimizes the cost function J, which is the optimal quadratic problem. The discrete state-space system is [47]:

$$\begin{cases} \dot{x}(k+1) = Ax(k) + Bu(k) \\ y(k) = Cx(k) + Du(k) \end{cases} \tag{3}$$

For each state, the optimal solution is:

$$u(k) = -K(k) = -R^{-1}B^T Px(k) \tag{4}$$

P is the only positive semi-definite matrix solution of the following Ricatti matrix equation [43]:

$$A^T P + PA - PBR^{-1}B^T P + Q = 0 \tag{5}$$

The system must be a priori observable and controllable. The purpose of this control is to reduce the cost function, which includes all state-space variables. The most significant benefit of using an LQR controller is that the system becomes asymptotically stable in a steady state.

Suppose the rank of the system matrix A is such that $rank\ (A)\ \leq\ 2$. In that case, it is necessary to increase the matrices (in terms of size or number) to complete state feedback control plus integral without altering the system characteristics. The augmented state-space model matrices are defined as [48]:

$$A_g = |A\ ;\quad -C| \tag{6}$$

$$A_h = |A_g\ ;\quad zero(n+1,1)| \tag{7}$$

$$B_h = |B\ ;\quad 0| \tag{8}$$

The optimal solution becomes:

$$u(k) = -K(k) = -R^{-1}{B_h}^T Px(k) \tag{9}$$

The Ricatti matrix becomes:

$${A_h}^T P + PA_h - PB_h R^{-1}{B_h}^T P + Q = 0 \tag{10}$$

The system must be a priori observable and controllable. The purpose of this control is to reduce the cost function, which includes all state-space variables. The most significant benefit of using an LQR controller is that the system becomes asymptotically stable in a steady state.

After the resolution of the cost function J, subject to (3) and the Ricatti matrix (10), an optimal K matrix is obtained with the augmented matrices, which defines all the control diagram constants shown in Fig. 2 [49].

$$K_i = K(1:n) \tag{11}$$

$$K_p = K(n+1) \tag{12}$$

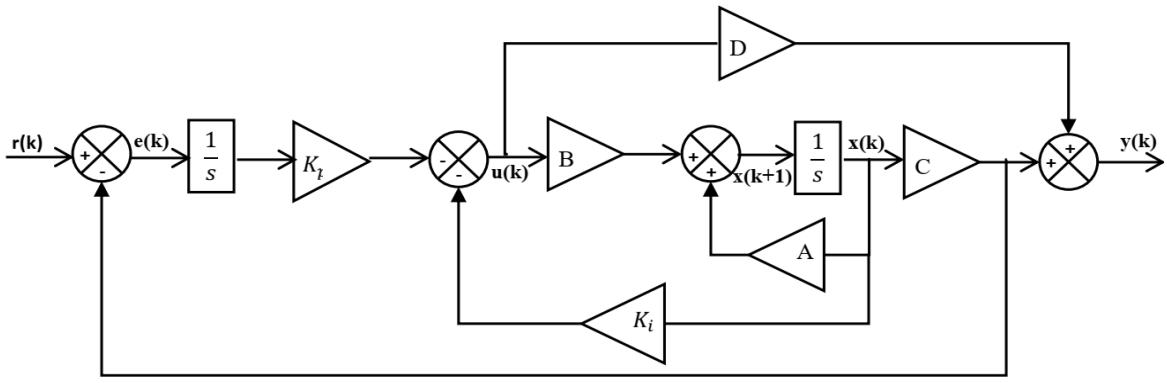

Fig. 2. Block diagram of LQR with integrator

3.2. Control of the HESS using LQR

The block diagram of the HESS control using LQR is shown in Fig. 3. The control strategy is based on decomposing the total current signal and implementing a low-pass filter [4]. Initially, the DC bus voltage V_{dc} is compared to the reference value V_{DC_ref}. The resulting error is then passed to the integrator and the K_{iv} controller. The latter generates the desired total current reference, I_{tot_ref}, to the ESS. This current is decomposed into a component of the low-frequency I_{LFC_ref} and a component of the high-frequency I_{HFC_ref}. The low-frequency part is given as follows [50]–[52]:

$$I_{LFC\_ref} = f_{LPF}(I_{tot\_ref}) \tag{13}$$

where f_{LPF} is the low-pass filter function.

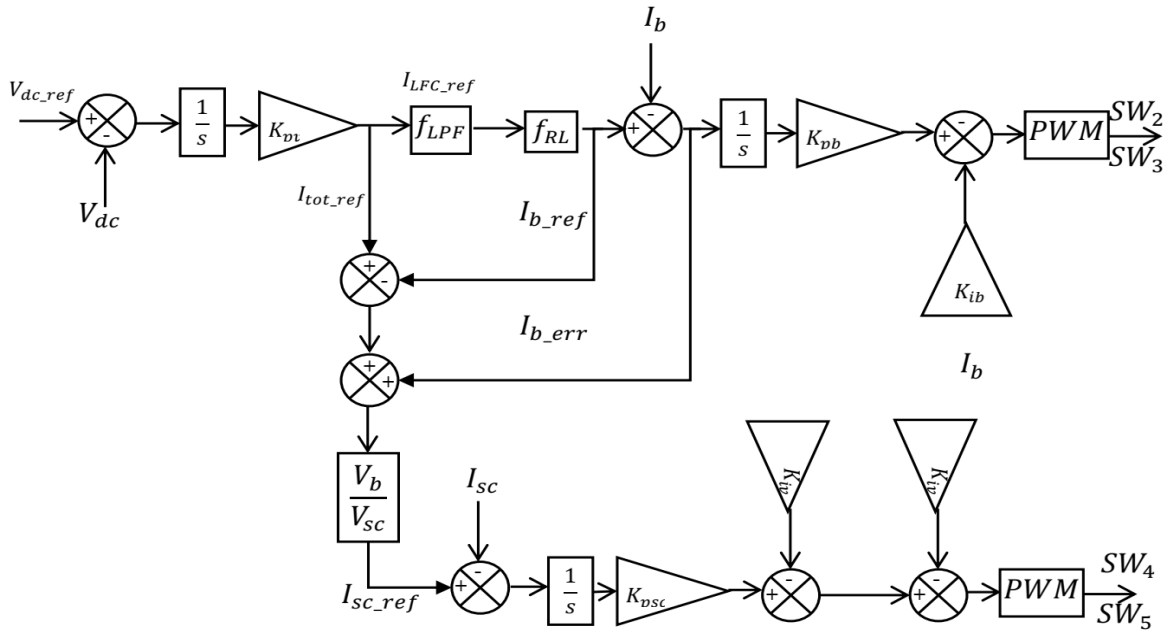

Fig. 3. HESS control using LQR

Since the energy storage system has a maximum charge and minimum discharge, it is necessary to control the charge/discharge of batteries by inserting a rate limiter, which provides the reference current to batteries as follows:

$$I_{b\_ref} = f_{RL}(I_{LFC\_ref}) \tag{14}$$

where f_{RL} is the rate limiter function.

After that, the battery reference current is compared to the battery measured current, and the difference is reported to the integrator and controller K_{ib}. The negative sum of (15) generates the duty ratio of the batteries, D_{bat}. Finally, to generate switching pulses for the battery switches (S_{w2} and S_{w3}), D_{bat} is delivered to the PWM generator [53].

$$D_{bat} = -I_{b\_err}\left(\frac{1}{s} + K_{pb}\right) - K_{pb}x \tag{15}$$

The high-frequency component is given as:

$$I_{HFC\_ref} = I_{tot\_ref} - I_{b\_ref} \tag{16}$$

Therefore, the uncompensated battery current I_{uc_b} is given as follows:

$$I_{uc\_b} = I_{HFC\_ref} + I_{b\_err} \tag{17}$$

The uncompensated battery power P_{uc_b} is given as follows:

$$P_{uc\_b} = I_{uc\_b} * V_b \tag{18}$$

The uncompensated battery power must be compensated by the supercapacitor, as indicated by the following equation:

$$P_{uc\_b} = I_{sc\_ref} * V_{sc} \tag{19}$$

where V_b and V_{sc} are the voltages of the batteries and the supercapacitor, respectively.

From (17), (18), and (19), the reference supercapacitor is given as follows:

$$I_{sc\_ref} = \left(I_{HFC_{ref}} + I_{b_{err}}\right) * \frac{V_b}{V_{sc}} \tag{20}$$

Similarly, the supercapacitor reference current is compared to the supercapacitor measured current. The difference is passed to the integrator and the controller K_{isc}. The negative sum of (22) generates the duty ratio of the supercapacitor D_{sc}. Lastly, to generate switching pulses for supercapacitor switches (S_{w4} and S_{w5}), D_{sc} is delivered to the PWM generator.

$$I_{sc\_err} = I_{sc\_ref} - I_{sc} \tag{21}$$

$$D_{sc} = -I_{sc\_err}\left(\frac{1}{s} + K_{psc}\right) - K_{psc}x \tag{22}$$

3.3. Design of Current LQR Control of SC

The state-space model of the supercapacitor is given by (23) and (24) [54]–[58].

$$\begin{vmatrix} \dot{I}_{sc} \\ \dot{V}_{dc} \end{vmatrix} = \begin{vmatrix} 0 & 1 \\ \frac{-(1-D_{sc})^2}{L_s C_f} & \frac{-1}{R_l C_f} \end{vmatrix} \begin{vmatrix} I_{sc} \\ V_{dc} \end{vmatrix} + \begin{vmatrix} 0 \\ \frac{1}{L_s C_f} \end{vmatrix} V_{sc} \tag{23}$$

$$V_{dc} = \left|\frac{2\,V_0}{R_l} \quad V_0 C_f\right| \left|\begin{matrix} I_{sc} \\ V_{dc} \end{matrix}\right| \tag{24}$$

where L_s is the inductance of the buck-boost converter of the supercapacitor, C_f is the DC bus capacitor, and R_l is the resistance of the load.

The state space matrices of the supercapacitor model become:

$$A_s = \left|\begin{matrix} 0 & 1 \\ \frac{-(1-D_{sc})^2}{L_s C_f} & \frac{-1}{R_l C_f} \end{matrix}\right|;\ B_s = \left|\begin{matrix} 0 \\ \frac{1}{L_s C_f} \end{matrix}\right|; C_s = \left|\frac{2\,V_0}{R_l} \quad V_0 C_f\right|;\ D_s = 0$$

Since the rank of A_s is $n = 2$, augmenting the matrices to complete the state feedback control plus integral without changing the system characteristics is necessary. The state space matrices of the supercapacitor model become:

$$A_g = |A_s; \quad -C_s| \tag{25}$$

$$A_{sc} = |A_g; \quad zero(3,1)| \tag{26}$$

$$B_{sc} = |B_s; \quad 0| \tag{27}$$

The optimal control law is written as follows:

$$u_{sc}(k) = -K_{sc}(k) = -{R_{sc}}^{-1} {B_{sc}}^T P_{sc} x_{sc}(k);\ k = 1,2,3 \tag{28}$$

The Ricatti matrix becomes:

$${A_{sc}}^T P_{sc} + P_{sc} A_{sc} - P_{sc} B_{sc} {R_{sc}}^{-1} {B_{sc}}^T P_{sc} + Q_{sc} = 0 \tag{29}$$

Following the resolution of the quadratic cost function J, subject to the state-space dynamics defined in (26) and (27) and the algebraic Riccati equation (29), the optimal state-feedback gain matrix K_{sc} was obtained using the augmented system matrices. This gain matrix encapsulates the feedback control gains necessary for implementing the LQR strategy, as depicted in the control block diagram of Fig. 2.

The gain matrix K_{sc} is structured as follows:

$$K_{isc} = K_{sc}(1{:}\,2) \tag{30}$$

$$K_{psc} = K_{sc}(3) \tag{31}$$

Here, K_{isc} corresponds to the feedback gains associated with the system states, while K_{psc} is the gain applied to the integrator state, ensuring proper regulation and improved steady-state performance. Through iterative simulation and tuning, the optimal weighting matrices for the LQR design were identified as:

$$Q = Diag(1,1,1); \quad R = 0.0001$$

These selected matrices reflect a design trade-off that places equal importance on the state variables while penalizing control effort modestly. The resulting controller provides a well-balanced dynamic response characterized by fast settling time, minimal overshoot, and negligible steady-state error, as validated by the transient performance data presented in Table 1.

Using MATLAB's LQR solver, the numerical solution for the optimal gain matrix K_{sc} was found to be: $K_{isc} = 10^5 * |0.0215 \quad -2.1476|$; $K_{psc} = -100.00$. These gain values serve as the control parameters for the LQR-based feedback controller in the HESS. They are directly applied in the system's real-time control implementation, as shown in the schematic of Fig. 6, enabling effective

regulation of the battery-supercapacitor power-sharing mechanism under varying operating conditions.

Table 1. Transient time characteristics for different values of Q and R

Q	R	Rise Time	Settling Time	Overshoot %	Steady-State Error
1	0.01	0.0283	0.0552	0	0.0014
1	0.001	0.0022	0.0195	1.61	1.61E-06
1	0.0001	0.0013	0.0034	4.99	1.03E-06
1	0.00001	7.50E-04	0.0021	4.29	9.42E-04
5	0.0001	8.46E-04	0.0025	4.27	4.01E-04
10	0.00001	7.50E-04	0.0021	4.29	9.42E-04

These matrices contain all the necessary data to assign the values of all LQR parameters in the control diagram shown in Fig. 4. It presents a detailed analysis of the supercapacitor current dynamics under various configurations of the LQR weighting matrices Q and R. The transient responses highlight how parameter tuning influences the control system's ability to swiftly and effectively suppress power fluctuations. Specifically, increased values of Q enhance the system's emphasis on state regulation, leading to faster convergence and reduced overshoot in the SC current, whereas variations in R modulate the control input magnitude, affecting system responsiveness and stability. This figure substantiates that optimal selection of these weighting matrices is crucial for achieving a balanced trade-off between rapid dynamic response and minimal energy exchange oscillations in the supercapacitor, ultimately augmenting the system's capacity to buffer transient power disturbances in renewable energy applications.

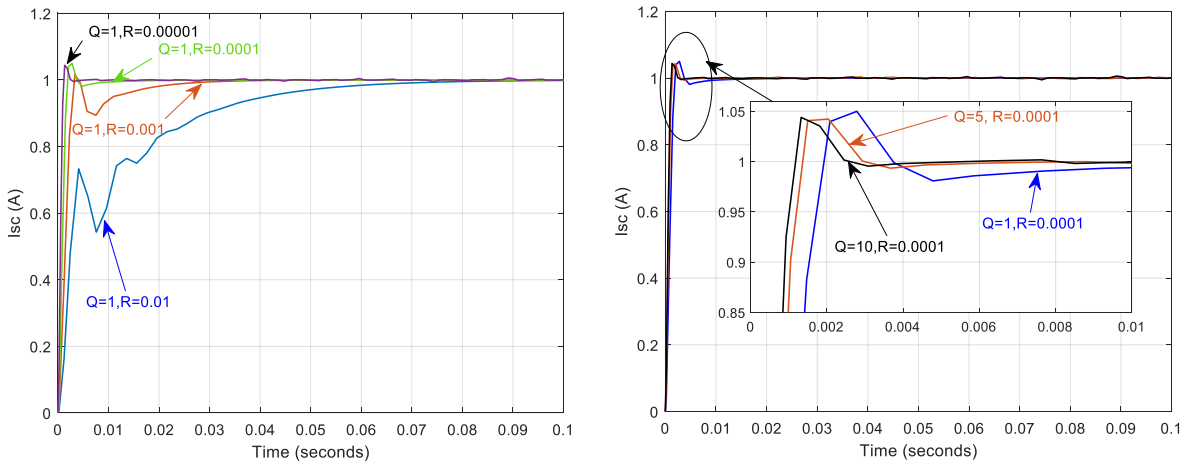

(a) (b)

Fig. 4. The transient responses of the SC current with (a) Q constant, R variable, (b) Q variable, R constant

Table 1 summarizes the transient time characteristics for different values of Q and R. As seen, the response time improves with a decrease in R. Additionally, the settling time is improved with a reduction in R, while the overshoot is enhanced with an increase in R. As seen, the response time improves with a decrease in R. Additionally, the settling time is improved with a reduction in R, while the overshoot is enhanced with an increase in R.

3.4. Design of Current LQR Control of Batteries

The state space model of the battery is given by the equations (32) and (33) [59], [60].

$$\begin{vmatrix} \dot{I}_b \\ \dot{V}_{dc} \end{vmatrix} = \begin{vmatrix} 0 & 1 \\ \frac{-(1-D_{bat})^2}{L_b C_f} & \frac{-1}{R_l C_f} \end{vmatrix} \begin{vmatrix} I_b \\ V_{dc} \end{vmatrix} + \begin{vmatrix} 0 \\ \frac{1}{L_b C_f} \end{vmatrix} V_b \tag{32}$$

$$V_{dc} = \left| \frac{2\,V_0}{R_l} \quad V_0 C_f \right| \left| \begin{matrix} I_b \\ V_{dc} \end{matrix} \right| \tag{33}$$

where L_b is the inductance of the buck-boost converter of the batteries; C_f is the DC bus capacitor; and R_l is the resistance of the load.

The state space matrices of the battery model become:

$$A_b = \left| \begin{matrix} 0 & 1 \\ \frac{-(1-D_b)^2}{L_b C_f} & \frac{-1}{R_l C_f} \end{matrix} \right|;\ B_b = \left| \begin{matrix} 0 \\ \frac{1}{L_b C_f} \end{matrix} \right|;\ C_b = \left| \frac{2\,V_0}{R_l} \quad V_0 C_f \right|;\ D_b = 0$$

Since the rank of A_b is $n = 2$, augmenting the matrices to complete the state feedback control plus integral without changing the system characteristics is necessary. The state space matrices of the supercapacitor model become:

$$A_{be1} = |A_b; \quad -C_b| \tag{34}$$

$$A_{be} = |A_{be1}; \quad zero(3,1)| \tag{35}$$

$$B_{be} = |B_b; \quad 0| \tag{36}$$

The optimal solution becomes:

$$u_{sc}(k) = -K_b(k) = -{R_b}^{-1} {B_b}^T P_b x_b(k);\ \ k = 1,2,3 \tag{37}$$

The Ricatti matrix becomes:

$${A_b}^T P_b + P_b A_b - P_b B_b {R_b}^{-1} {B_b}^T P_b + Q_b = 0 \tag{38}$$

After the resolution of the cost function J, subject to (35), (36), and the Ricatti matrix (38), an optimal matrix K_b is obtained with augmented matrices, which define all the constants of the control diagram shown in Fig. 5.

$$K_{ib} = K_b(1{:}2) \tag{39}$$

$$K_{pb} = K_b(3) \tag{40}$$

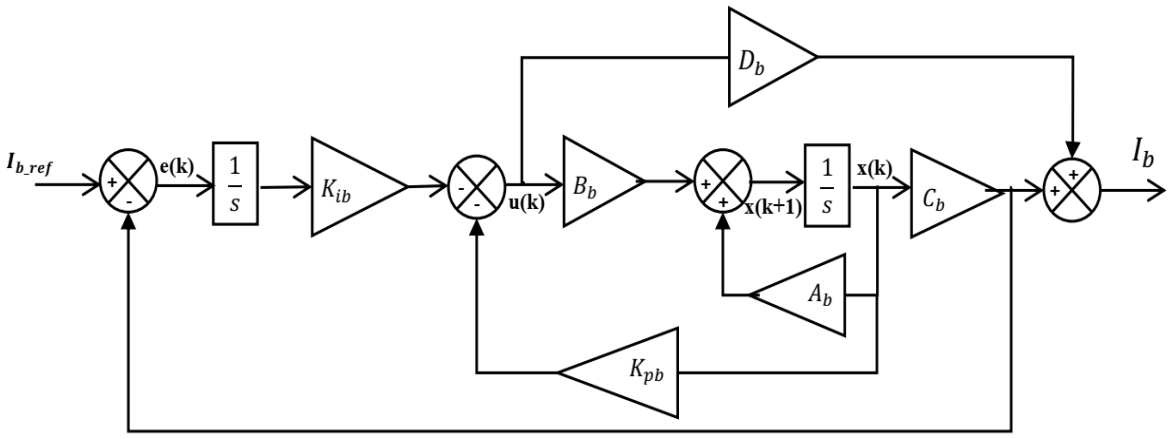

Fig. 5. The batteries are controlled using LQR

Similarly, after numerous simulations, the estimated best values for matrices Q and R are: $Q = diag(|5 \quad 5 \quad 5|$ and $R = 0.01$. These parameters enable the system to exhibit good performance, characterized by smooth and quick transitory reactions, low overshoot, low steady-state error, and

stability. Using a MATLAB program to solve the LQR problem for K_b: $K_{ib} = 10^5 * |0.0086 \quad -1.0616|$, and $K_{pb} = -22.3607$.

3.5. Design of Current LQR Control of HESS

The state-space model of the voltage control from the supercapacitor's inductor current to the output voltage is given by [61]–[63]:

$$\dot{V}_{dc} = \frac{-2}{R_f C_f} V_0 + \frac{1}{R_f C_f} V_{sc} \tag{41}$$

$$I_{sc} = \frac{2L_s + {R_f}^2 C_f (1 - D_{sc})^2}{(1 - D_{sc}) R_f C_f} V_0 + \frac{L_s}{R_f C_f (1 - D_{sc})} V_{sc} \tag{42}$$

The state space matrices of the battery model become:

$$A_v = \frac{-2}{R_f C_f}\,;\; B_v = \frac{1}{R_f C_f}\,;\; C_v = \frac{2L_s + {R_f}^2 C_f (1-D_{sc})^2}{(1-D_{sc}) R_f C_f}\,;\; D_v = \frac{L_s}{R_f C_f (1-D_{sc})}$$

Since the $n = 1$ rank of A_v, it is necessary to augment the matrices for complete state feedback control plus integral without altering the system characteristics. The state-space matrices of the voltage control model become:

$$A_{v1} = |A_v\,; \quad -C_v| \tag{43}$$

$$A_{v2} = |A_{v1}\,; \quad zero(2,1)| \tag{44}$$

$$B_{v1} = |B_v\,; \quad 0| \tag{45}$$

The optimal solution becomes:

$$u_v(k) = -K_v(k) = -{R_v}^{-1} {B_v}^T P_v x_v(k)\,; \;\; k = 1,2 \tag{46}$$

The Ricatti matrix becomes:

$${A_v}^T P_v + P_v A_v - P_v B_v {R_v}^{-1} {B_v}^T P_v + Q_v = 0 \tag{47}$$

After the resolution of the cost function J, subject to (43), (44), and the Ricatti matrix (47), an optimal matrix K_v is obtained with augmented matrices, which define all the constants of the control diagram shown in Fig. 6.

$$K_{iv} = K_b(1) \tag{48}$$

$$K_{pv} = K_b(2) \tag{49}$$

After numerous simulations, as shown in Fig. 7, the estimated best values for matrices Q and R are: $Q = diag(|1 \quad 1|)$ and $R = 0.0001$.

These parameters enable the system to exhibit good performance, characterized by smooth and quick transitory reactions, low overshoot, low steady-state error, and stability, as shown in Table 2. Using a MATLAB program to solve the LQR problem for K_v: $K_{iv} = 441.1724$, and $K_{pv} = -100.00$. These matrices contain all of the data needed to complete the LQR control diagram in Fig. 7.

Fig. 7 exemplifies the efficacy of the LQR-based voltage control strategy in maintaining the stability of the DC bus voltage under conditions of significant load variability and fluctuating solar irradiance. The plotted waveform illustrates that, despite dynamic changes in load demand, the control scheme consistently sustains the bus voltage within a tight proximity to its predetermined reference,

reflecting high control precision and robustness. The rapid response to transient disturbances underscores the controller's capacity to adaptively modulate power exchanges between the energy storage components and the PV generation source, ensuring a resilient and reliable power supply in the face of renewable intermittency and load uncertainty, which are inherent challenges in sustainable microgrid operation. Table 2 summarizes the transient time characteristics for different values of Q and R.

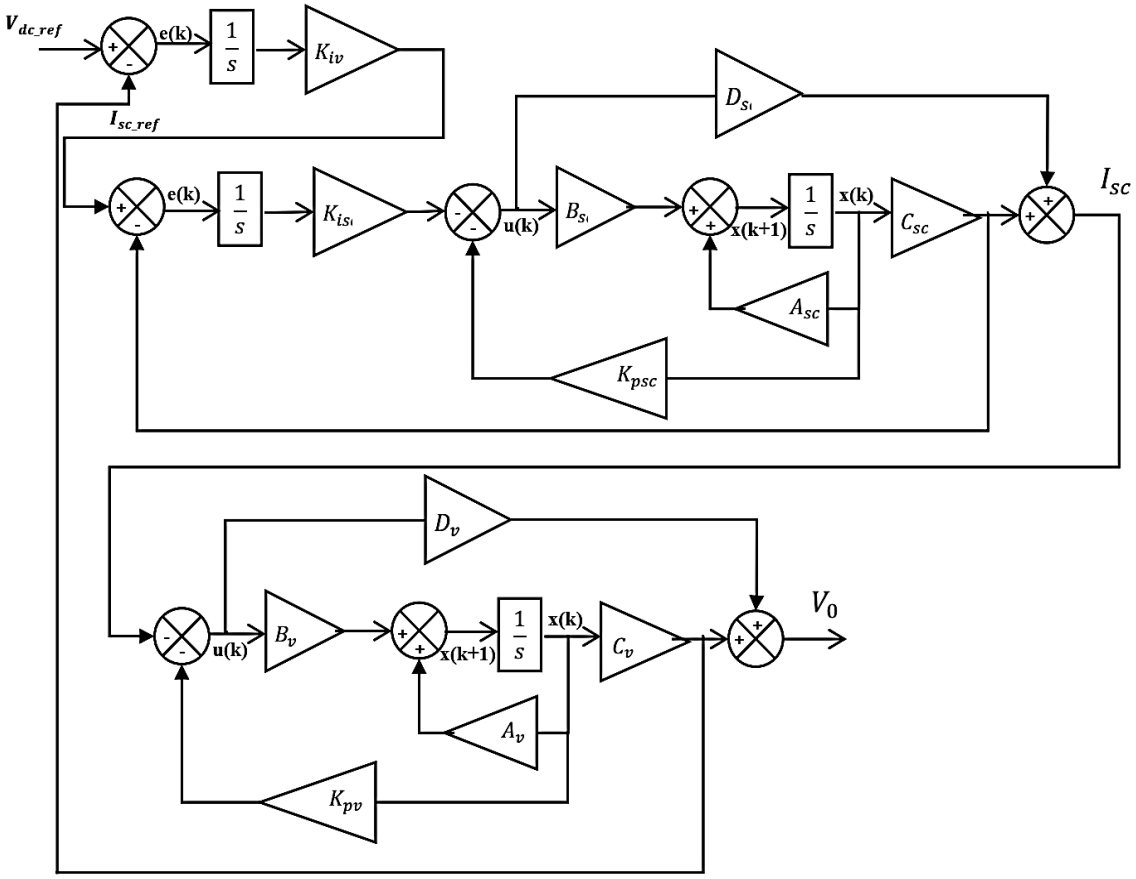

Fig. 6. The voltage and supercapacitor control using LQR

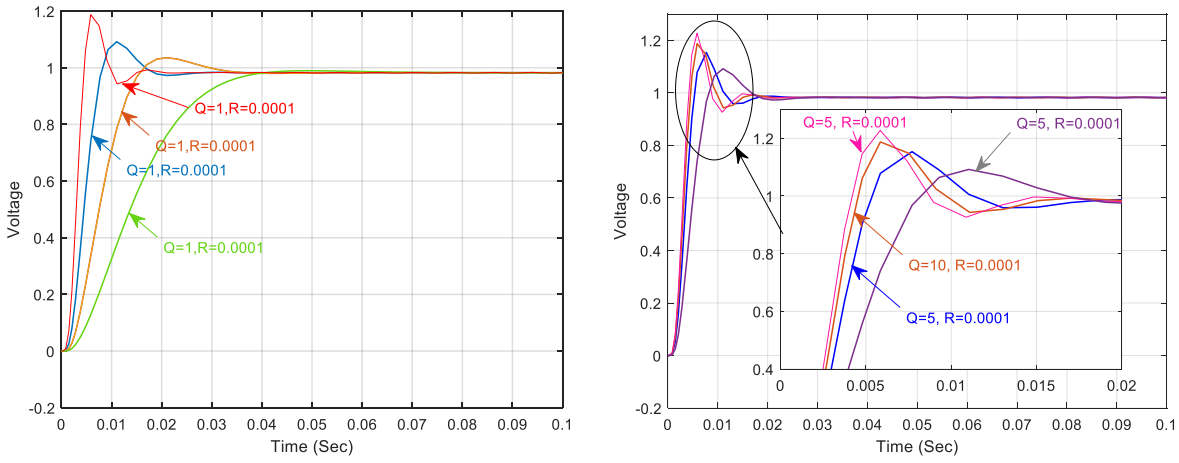

(a) (b)

Fig. 7. The transient responses of the voltage control with: (a) Q constant, R variable; (b) Q variable, R constant

Table 2. The transient time characteristics for different values of Q and R for voltage DC bus control using LQR

Q	R	Rise time	Settling time	Over shoot %	ss_error
1	0.00001	0.002493	0.9814	21.34%	0.0177
1	0.0001	0.0048	0.0166	11.1381	0.0175
1	0.001	0.2729	0.9825	0	0.0175
1	0.01	0.6571	0.9825	0	0.0175
5	0.0001	0.002962	0.9819	17.059	0.0179
10	0.0001	0.002493	0.9814	21.34	0.0172
15	0.0001	0.00332	0.9828	24.375	0.019

4. Simulated Results

The LQR controller designed in the previous section for the standalone PV system with hybrid storage (illustrated in Fig. 1) was evaluated through two distinct simulation scenarios implemented in MATLAB/Simulink and compared with the PI classic controller. In the first scenario, solar irradiation was held constant at 800 W/m², while a variable load profile was applied, enabling an assessment of the controller's responsiveness to dynamic power demand. In the second scenario, a constant load was maintained while solar irradiation varied, allowing evaluation of the controller's ability to adapt to changing PV generation conditions.

4.1. Scenario 1: Variable Load and Constant Solar Irradiance

The solar irradiance was fixed at 800 W/m², and the load varied between the minimum value (200 W) and the maximum (1200 W), as shown in Fig. 8(a). The power generated by the PV source is P_{pv} = 790 W. The waveforms of the different power sources, including the supercapacitor and batteries, are shown in Fig. 8 (b). The voltage of the DC bus is equal to V_{DC} = 48 V, as shown in Fig. 8(b). Fig. 8(a) and Fig. 8(b) compare the two classic PID controllers and the LQR controller for variations in PV power and load power. It can be observed that at t = 1, 2, and 3 seconds, there are load fluctuations. This figure depicts the dynamic interplay of power flows between the PV source and load under a loaded operational scenario with constant solar irradiance.

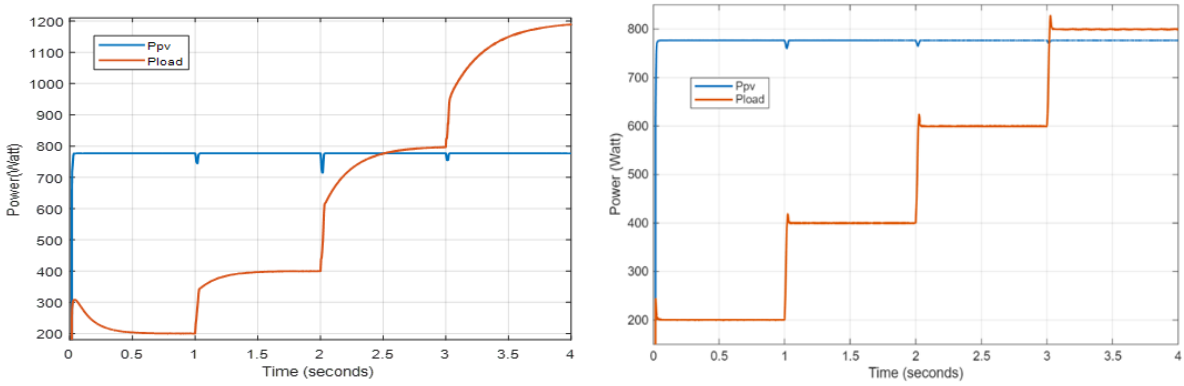

(a) (b)

Fig. 8. Simulation of the HESS under variable load P_{pv} and P_{load} : (a) with PI controller; (b) with LQR controller

Fig. 9(a) and Fig. 9(b) compare the two classic PID controllers and the LQR for the variation of battery power and supercapacitor power. It can be observed that at $t = 1, 2, \text{and } 3$ seconds, there are load fluctuations. The supercapacitor mitigates these fluctuations. During the dynamic regime, the batteries continue to charge (when $P_{pv} > P_{load}$) or discharge (when $P_{pv} < P_{load}$) energy as appropriate. Also, it can be observed that the battery management is better for the LQR controller than the PI controller.

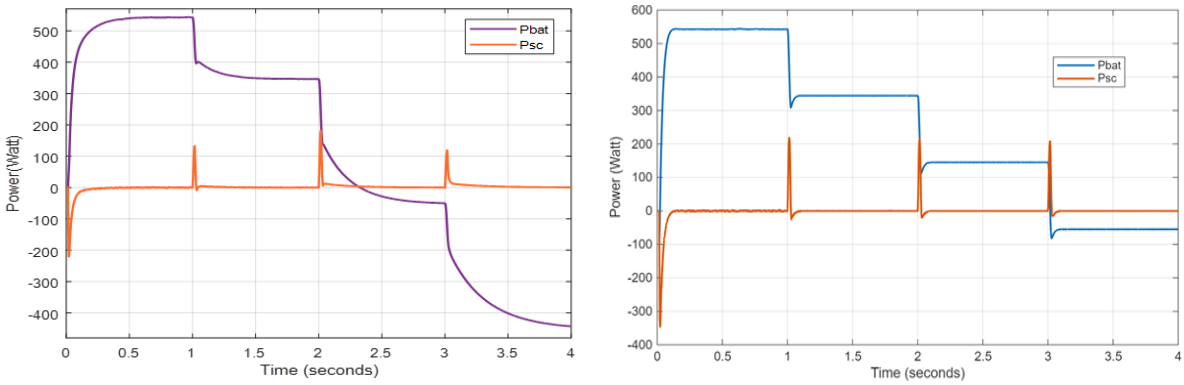

(a) (b)

Fig. 9. Simulation of the HESS under variable load P_{sc} and P_{bat} : (a) with PI controller, (b) with LQR controller

Fig. 10(a) and Fig. 10(b) compare both controllers for the DC bus voltage under the fluctuation of the load. It is clear that Fig. 10(b) is much more stable than the first. The LQR controller gives much better results than the classic PI controller under variable load.

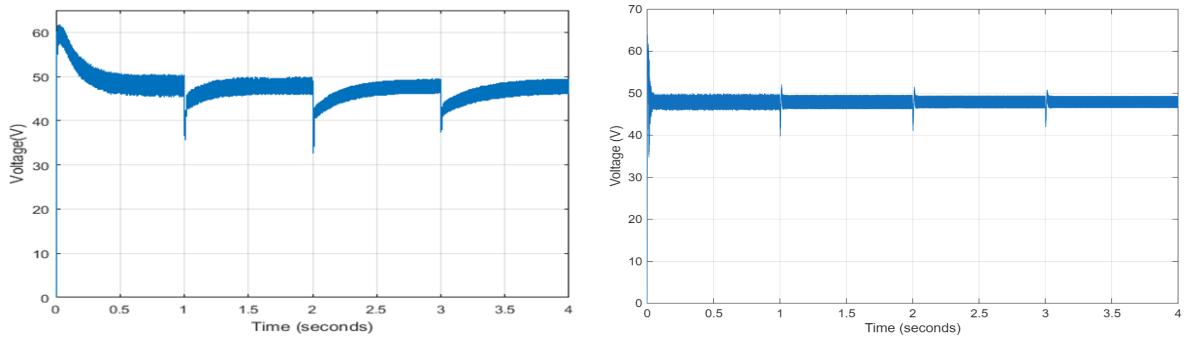

(a) (b)

Fig. 10. Simulation of the HESS under variable load DC bus voltage: (a) with PI controller; (b) with LQR controller

The graphical data demonstrate the system's energy management, in which the supercapacitor rapidly absorbs transient power surges to mitigate fluctuations, thereby providing fast-response buffering. Concurrently, the battery supplies or absorbs energy to address sustained power imbalances, facilitating efficient energy utilization and stabilizing the DC bus voltage. This coordinated energy management exemplifies the effectiveness of the LQR controller in optimizing power sharing, minimizing pulsations, and enhancing overall stability, which are crucial for ensuring the reliable operation of RESs under variable conditions. And, it's better than the PI controller.

4.2. Scenario 2: Constant Load and Variable Solar Irradiance

The second scenario is performed under different solar irradiation values (800 W/m², 700 W/m², 600 W/m², 500 W/m²), as shown in Fig. 11.

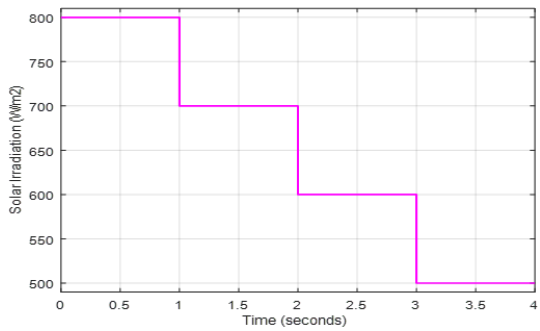

Fig. 11. Simulation of the HESS under variable irradiance: Solar irradiance

Fig. 12(a) and Fig. 12(b) present the variation of Ppv and Pload for both controllers, the PI classic and the LQR controller. It can be observed that the load variation is more stable for the LQR controller than the PI controller.

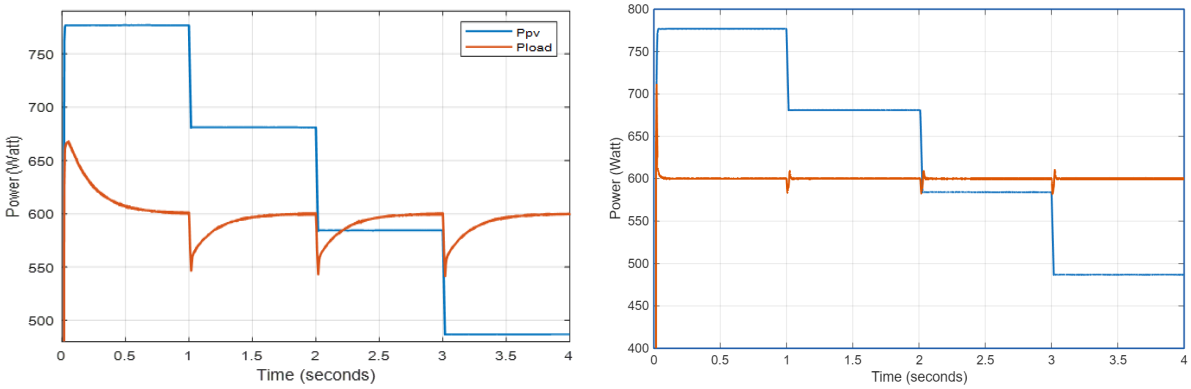

(a) (b)

Fig. 12. Simulation of the HESS under variable irradiance P_{pv} and P_{load}: (a) with PI controller; (b) with LQR controller

Fig. 13(a) and Fig. 13(b) compare the variation of power batteries and supercapacitors. It can be observed that, from $t = 0\ s$ to 1 s, the PV power is; the battery entirely supports the load. Next, the battery power fluctuates in response to variations in PV power. If the available power is insufficient, the battery is in its discharge phase to provide the required power. Otherwise, if there is a surplus of PV power, the battery operates in charging mode, storing the excess PV generation for later use. Then, the supercapacitor mitigates power source fluctuations, as seen at $t = 1, 2,$ and 3 s. Also, the LQR controller yields better results, especially in battery management.

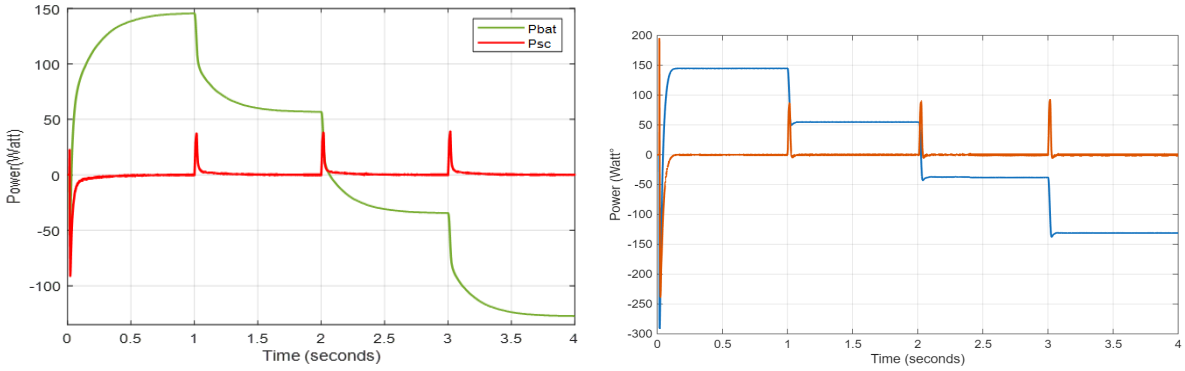

(a) (b)

Fig. 13. Simulation of the HESS under variable irradiance P_{sc} and P_{bat}: (a) PI controller; (b) LQR controller

Fig. 14(a) and Fig. 14(b) compare both controllers for the DC bus voltage under variable solar irradiance. It is clear that Fig. 14(b) is much more stable than Fig. 14(a); the LQR controller yields much better results than the classic PI controller under variable solar irradiance.

These figures provide a comprehensive simulation assessment of the HESS's response to fluctuating solar irradiance, thereby evaluating the efficacy of the proposed control scheme under realistic renewable energy sourcing scenarios. The data reveal that, as solar irradiance varies significantly, the LQR control strategy effectively maintains the DC bus voltage near its setpoint, demonstrating robust voltage regulation amid input fluctuations, and it's better than the PI controller. The power flow analysis demonstrates that the supercapacitor dynamically compensates for rapid surges and dips in PV power, effectively smoothing transient energy fluctuations. Meanwhile, the battery adjusts its charge-discharge behavior to accommodate longer-term energy variations. These findings underscore the control system's capacity to sustain stable, reliable operation in renewable-dominant microgrids, effectively mitigating the adverse effects of intermittent solar radiation.

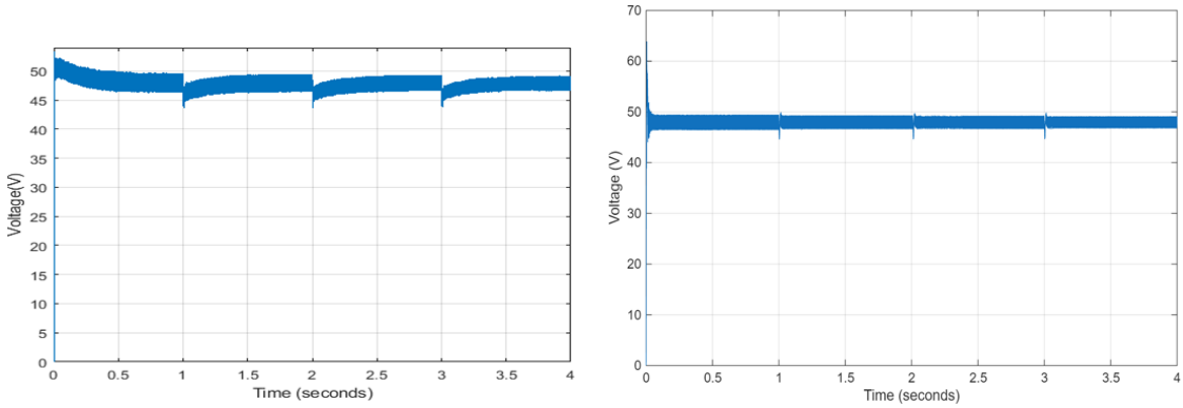

(a) (b)

Fig. 14. Simulation of the HESS under variable irradiance DC bus voltage: (a) with PI controller; (b) with LQR controller.

5. Conclusion

This study demonstrates the effectiveness of the LQR for robust, optimal control of hybrid energy storage systems in photovoltaic microgrids. Compared with the PI classic controller, the LQR approach offers several distinct advantages. Primarily, it offers a systematic and principled framework for balancing the competing objectives of rapid response and control effort via adjustable weighting matrices, thereby enhancing system stability and adaptability. Additionally, the LQR guarantees a globally optimal solution by minimizing a quadratic cost function, resulting in superior dynamic performance and robustness against parameter variations and external disturbances. Its straightforward design procedure, free of the complexities associated with pole assignment, facilitates easier implementation and scalability in real-world microgrid applications. Overall, the LQR-based control strategy significantly improves power fluctuation attenuation, response speed, and system reliability, making it a preferable choice for advanced energy management in renewable-integrated microgrids over conventional pole-placement methods. In light of these outcomes, future research avenues include experimental validation of the control framework in real-world settings, adaptive tuning strategies for system parameters in response to unforeseen disturbances, and the integration of advanced predictive algorithms to enhance system resilience and operational efficiency further. Overall, this work contributes valuable insights into the development of intelligent, reliable, and sustainable energy management systems for next-generation microgrids.

Sustainable Development Goals: Sustainable Development Goals mapped to this document, Affordable and Clean Energy Goal 7.

Data Availability: The data used to support the findings of this study are available at reasonable request from the corresponding author.

Author Contribution: All authors contributed equally to the main contributor to this paper. All authors read and approved the final paper.

Funding: The authors extend their appreciation to the Northern Border University, Saudi Arabia for supporting this work through project number "NBU-CRP-2026-2448". Also, This article has been produced with the financial support of the European Union under the REFRESH—Research Excellence For REgion Sustainability and High-tech Industries project number CZ.10.03.01/00/22_003/0000048 via the Operational Programme Just Transition.

Acknowledgment: The authors extend their appreciation to the Northern Border University, Saudi Arabia for supporting this work through project number "NBU-CRP-2026-2448". Also, This article has been produced with the financial support of the European Union under the REFRESH—Research Excellence For REgion Sustainability and High-tech Industries project number CZ.10.03.01/00/22_003/0000048 via the Operational Programme Just Transition.

Conflicts of Interest: The authors declare that they have no conflicts of interest.

List of Abbreviations

RESs	Renewable energy sources
ESSs	Energy storage systems
HESSs	Hybrid ESSs
FLC	Fuzzy logic control
SMC	Sliding mode control
EVs	Electric vehicles
V2G	Vehicle-to-grid
PQ	Power quality
R_l	The load resistance, Ω
I_{pv}	Photovoltaic panel current, A
I_{sc}	Supercapacitor current, A
V_b	Battery voltage, V
C_f	The filter capacitance, F
MGs	Microgrids
f_{LPF}	The low-pass filter function
D_{bat}	The duty ratio of batteries
f_{RL}	The rate limiter function
V_{dc}	The DC bus voltage, V
WP	Wind power
I_b	Battery current, A
PV	Photovoltaic
P_{bat}	The power of the batteries, W
P_{pv}	The power of the PV source, W
P_{sc}	The power of the supercapacitor, W
LQR	Linear Quadratic Regulator
L_{pv}	The filter of the boost converter, H
RB-EMS	Rule-based energy management system
D-MPC	Dual-model predictive control
SMES	Superconducting magnetic energy storage
SOC	State of charge
PWM	Pulse width modulation
D_{sc}	The duty ratio of the supercapacitor
V_{pv}	Photovoltaic panel voltage, V
V_{sc}	Supercapacitor voltage, V
L_{sc}	The filter of the supercapacitor buck-boost converter, H
MPPT	Maximum power point tracking
I_{LFC_ref}	The low-frequency reference current, A
L_b	The filter of the battery buck-boost converter, H
I_{HFC_ref}	The high frequency reference current, A
I_{b_ref}	Batteries reference current, A

I_{tot_ref}	The total reference current for ESS, A
V_{dc_ref}	The DC bus reference voltage, V
P_{load}	The power consumed by the load, W

References

[1] D. Choi, D. Kim, and J. D. Turner, "Optimization of weight matrices for the linear quadratic regulator problem using algebraic closed-form solutions," *Electronics*, vol. 12, no. 21, p. 4526, 2023, https://doi.org/10.3390/electronics12214526.

[2] M. Awad, A. Said, M. H. Saad, A. Farouk, M. M. Mahmoud, M. S. Alshammari, M. L. Alghaythi, S. H. E. Abdel Aleem, A. Y. Abdelaziz, and A. I. Omar, "A review of water electrolysis for green hydrogen generation considering PV/wind/hybrid/hydropower/geothermal/tidal and wave/biogas energy systems, economic analysis, and its application," *Alexandria Engineering Journal*, vol. 87, pp. 213–239, 2024, https://doi.org/10.1016/j.aej.2023.12.032.

[3] N. F. Ibrahim, M. M. Mahmoud, A. M. H. A. Thaiban, A. B. Barnawi, Z. M. S. Elbarbary, A. I. Omar, and H. Abdelfattah, "Operation of grid-connected PV system with ANN-based MPPT and an optimized LCL filter using GRG algorithm for enhanced power quality," *IEEE Access*, vol. 11, pp. 106859–106876, 2023, https://doi.org/10.1109/ACCESS.2023.3317980.

[4] N. S. Santarisi and S. S. Faouri, "Prediction of combined cycle power plant electrical output power using machine learning regression algorithms," *Eastern-European Journal of Enterprise Technologies*, vol. 6, no. 8(114), pp. 16–26, 2021, https://doi.org/10.15587/1729-4061.2021.245663.

[5] M. Aljaidi, P. Jangir, Arpita, S. P. Agrawal, S. B. Pandya, A. Parmar, A. F. Alkoradees, R. Jangid, and T. R. Agrawal, "A novel educational competition optimizer for precise parameter optimization in proton exchange membrane fuel cells," *Ionics*, vol. 31, no. 10, pp. 10777–10803, 2025, https://doi.org/10.1007/s11581-025-06568-8.

[6] A. Ahmad, A. Raza, M. Farman, A. Akgül, M. Nauman Aslam, D. Baleanu, S. A. O. Abdallah, and N. S. Abd El-Gawaad, "Flip bifurcation and numerical study of Crimean–Congo hemorrhagic fever with sustainable fractional approach," *Fractals*, vol. 34, no. 4, p. 2540057, 2025, https://doi.org/10.1142/S0218348X25400572.

[7] S. J. Daniel, M. Karpagam, A. Flah, and S. Ben Chaabane, "Power quality improvement and energy management in hybrid microgrids using a dual-optimization approach," *Scientific Reports*, vol. 15, no. 1, p. 36201, 2025, https://doi.org/10.1038/s41598-025-20001-0.

[8] S. V. V. N. Chanukya Padira, H. Javvaji, Z. Parvez, K. Sarada, B. H. Kumar, and A. R. Singh, "A switched capacitor–inductor high gain DC-DC converter for solar PV applications," *International Journal of Energy and Environment Research*, vol. 13, no. 1, pp. 101–107, 2025, https://doi.org/10.37391/IJEER.130114.

[9] O. O. Yolcan, "World energy outlook and state of renewable energy: 10-year evaluation," *Innovation and Green Development*, vol. 2, no. 4, p. 100070, 2023, https://doi.org/10.1016/j.igd.2023.100070.

[10] M. M. Mahmoud, B. S. Atia, Y. M. Esmail, S. A. E. M. Ardjoun, N. Anwer, A. I. Omar, F. Alsaif, S. Alsulamy, and S. A. Mohamed, "Application of whale optimization algorithm based FOPI controllers for STATCOM and UPQC to mitigate harmonics and voltage instability in modern distribution power grids," *Axioms*, vol. 12, no. 5, p. 420, 2023, https://doi.org/10.3390/axioms12050420.

[11] S. Vadivel and U. S. Ragupathy, "Modeling and design of high performance converters for optimal utilization of interconnected renewable energy resources to micro grid with GOLRS controller," *International Journal of Control, Automation and Systems*, vol. 19, no. 1, pp. 63–75, 2021, https://doi.org/10.1007/s12555-019-0498-2.

[12] F. Menzri, T. Boutabba, I. Benlaloui, H. Bawayan, M. I. Mosaad, and M. M. Mahmoud, "Applications of hybrid SMC and FLC for augmentation of MPPT method in a wind-PV-battery configuration," *Wind Engineering*, vol. 48, no. 6, pp. 1186–1202, 2024, https://doi.org/10.1177/0309524X241254364.

[13] P. Sinha, K. Paul, I. M. Elzein, M. M. Mahmoud, A. M. El-Rifaie, W. F. Mbasso, and A. M. Ewais, "Classifying power quality issues in railway electrification systems using a nonsubsampled contourlet transform approach," *Engineering Reports*, vol. 7, no. 8, p. e70301, 2025, https://doi.org/10.1002/eng2.70301.

[14] D. Rekioua, "Energy storage systems for photovoltaic and wind systems: A review," *Energies*, vol. 16, no. 9, p. 3893, 2023, https://doi.org/10.3390/en16093893.

[15] M. M. Hussein, T. H. Mohamed, M. M. Mahmoud, M. Aljohania, M. I. Mosaad, and A. M. Hassan, "Regulation of multi-area power system load frequency in presence of V2G scheme," *PLOS ONE*, vol. 18, no. 9, p. e0291463, 2023, https://doi.org/10.1371/journal.pone.0291463.

[16] O. M. Lamine, N. Bessous, B. Abdelhalim, F. A. Banakhr, M. I. Mosaad, O. Mammeri, and M. M. Mahmoud, "A combination of INC and fuzzy logic-based variable step size for enhancing MPPT of PV systems," *International Journal of Robotics and Control Systems*, vol. 4, no. 2, pp. 877–892, 2024, https://doi.org/10.31763/ijrcs.v4i2.1428.

[17] M. S. Wasim, S. Habib, M. Amjad, A. R. Bhatti, E. M. Ahmed, and M. A. Qureshi, "Battery-ultracapacitor hybrid energy storage system to increase battery life under pulse loads," *IEEE Access*, vol. 10, pp. 62173–62182, 2022, https://doi.org/10.1109/ACCESS.2022.3182468.

[18] N. Benalia, I. Benlaloui, K. Laroussi, A. Elkhateb, D. E. M. Wapet, A. M. Hassan, and M. M. Mahmoud, "Correction: Enhancing electric vehicle charging performance through series-series topology resonance-coupled wireless power transfer," *PLOS ONE*, vol. 19, no. 8, p. e0309545, 2024, https://doi.org/10.1371/journal.pone.0309545.

[19] T. S. Babu, K. R. Vasudevan, V. K. Ramachandaramurthy, S. B. Sani, S. Chemud, and R. M. Lajim, "A comprehensive review of hybrid energy storage systems: Converter topologies, control strategies and future prospects," *IEEE Access*, vol. 8, pp. 148702–148721, 2020, https://doi.org/10.1109/ACCESS.2020.3015919.

[20] M. M. Mahmoud, H. S. Salama, M. M. Aly, and A. M. M. Abdel-Rahim, "Design and implementation of FLC system for fault ride-through capability enhancement in PMSG-wind systems," *Wind Engineering*, vol. 45, no. 5, pp. 1361–1373, 2021, https://doi.org/10.1177/0309524X20981773.

[21] R. Kandari, N. Neeraj, and A. Micallef, "Review on recent strategies for integrating energy storage systems in microgrids," *Energies*, vol. 16, no. 1, p. 317, 2023, https://doi.org/10.3390/en16010317.

[22] M. M. Mahmoud, M. K. Ratib, M. M. Aly, and A. M. M. Abdel-Rahim, "Application of whale optimization technique for evaluating the performance of wind-driven PMSG under harsh operating events," *Process Integration and Optimization for Sustainability*, vol. 6, no. 2, pp. 447–470, 2022, https://doi.org/10.1007/s41660-022-00224-8.

[23] A. Dutta, S. Mitra, M. Basak, and T. Banerjee, "A comprehensive review on batteries and supercapacitors: Development and challenges since their inception," *Energy Storage*, vol. 5, no. 1, p. e339, 2023, https://doi.org/10.1002/est2.339.

[24] A. T. Hassan, F. A. Banakhr, M. M. Mahmoud, M. I. Mosaad, A. F. Rashwan, M. R. Mosa, M. M. Hussein, and T. H. Mohamed, "Adaptive load frequency control in microgrids considering PV sources and EVs impacts: Applications of hybrid sine cosine optimizer and balloon effect identifier algorithms," *International Journal of Robotics and Control Systems*, vol. 4, no. 2, pp. 941–957, 2024, https://doi.org/10.31763/ijrcs.v4i2.1448.

[25] O. M. Kamel, I. Elzein, M. M. Mahmoud, A. Y. Abdelaziz, M. M. Hussein, and A. A. Z. Diab, "Effective energy management strategy with a novel design of fuzzy logic and JAYA-based controllers in isolated DC/AC microgrids: A comparative analysis," *Wind Engineering*, vol. 49, no. 1, pp. 199–222, 2025, https://doi.org/10.1177/0309524X241263518.

[26] X. Lin and R. Zamora, "Controls of hybrid energy storage systems in microgrids: Critical review, case study and future trends," *Journal of Energy Storage*, vol. 47, p. 103884, 2022, https://doi.org/10.1016/j.est.2021.103884.

[27] K. Sayed, S. Abdel-Khalek, H. M. H. Zakaly, and M. Aref, "Energy management and control in multiple storage energy units (battery–supercapacitor) of fuel cell electric vehicles," *Materials*, vol. 15, no. 24, p. 8932, 2022, https://doi.org/10.3390/ma15248932.

[28] Y. Xin, J. Hu, and Z. Wang, "An energy management strategy with considering ultracapacitor ideal state of charge for fuel cell/battery/ultracapacitor vehicle," *Energy*, vol. 304, p. 132024, 2024, https://doi.org/10.1016/j.energy.2024.132024.

[29] Z. Cabrane, J. Kim, K. Yoo, and M. Ouassaid, "HESS-based photovoltaic/batteries/supercapacitors: Energy management strategy and DC bus voltage stabilization," *Solar Energy*, vol. 216, pp. 551–563, 2021, https://doi.org/10.1016/j.solener.2021.01.048.

[30] A. A. Kamel, H. Rezk, and M. A. Abdelkareem, "Enhancing the operation of fuel cell-photovoltaic-battery-supercapacitor renewable system through a hybrid energy management strategy," *International Journal of Hydrogen Energy*, vol. 46, no. 8, pp. 6061–6075, 2021, https://doi.org/10.1016/j.ijhydene.2020.06.052.

[31] M. M. Gulzar, A. Iqbal, D. Sibtain, and M. Khalid, "An innovative converterless solar PV control strategy for a grid connected hybrid PV/wind/fuel-cell system coupled with battery energy storage," *IEEE Access*, vol. 11, pp. 23245–23259, 2023, https://doi.org/10.1109/ACCESS.2023.3252891.

[32] P. Singh and J. S. Lather, "Dynamic power management and control for low voltage DC microgrid with hybrid energy storage system using hybrid bat search algorithm and artificial neural network," *Journal of Energy Storage*, vol. 32, p. 101974, 2020, https://doi.org/10.1016/j.est.2020.101974.

[33] A. Mahmoudian, R. Garmabdari, F. Bai, J. M. Guerrero, M. Mousavizade, and J. Lu, "Adaptive power-sharing strategy in hybrid AC/DC microgrid for enhancing voltage and frequency regulation," *International Journal of Electrical Power & Energy Systems*, vol. 156, p. 109696, 2024, https://doi.org/10.1016/j.ijepes.2023.109696.

[34] H. Maghfiroh, O. Wahyunggoro, and A. I. Cahyadi, "Energy management in hybrid electric and hybrid energy storage system vehicles: A fuzzy logic controller review," *IEEE Access*, vol. 12, pp. 56097–56109, 2024, https://doi.org/10.1109/ACCESS.2024.3390436.

[35] Z. Liu, A. Mohammadzadeh, H. Turabieh, M. Mafarja, S. S. Band, and A. Mosavi, "A new online learned interval type-3 fuzzy control system for solar energy management systems," *IEEE Access*, vol. 9, pp. 10498–10508, 2021, https://doi.org/10.1109/ACCESS.2021.3049301.

[36] X. Lu, W. Liao, W. Huang, Y. Xu, and X. Chen, "An improved linear quadratic regulator control method through convolutional neural network–based vibration identification," *Journal of Vibration and Control*, vol. 27, no. 7–8, pp. 839–853, 2021, https://doi.org/10.1177/1077546320933756.

[37] K. Zielonacki and J. Tarnawski, "PLC-based implementation of stochastic optimization method in the form of evolutionary strategies for PID, LQR, and MPC control," *International Journal of Control, Automation and Systems*, vol. 22, no. 6, pp. 1846–1855, 2024, https://doi.org/10.1007/s12555-023-0869-6.

[38] J. Duan, W. Cao, Y. Zheng, and L. Zhao, "On the optimization landscape of dynamic output feedback linear quadratic control," *IEEE Transactions on Automatic Control*, vol. 69, no. 2, pp. 920–935, 2024, https://doi.org/10.1109/TAC.2023.3275732.

[39] J. Rocabert, R. Capó-Misut, R. S. Muñoz-Aguilar, J. I. Candela, and P. Rodriguez, "Control of energy storage system integrating electrochemical batteries and supercapacitors for grid-connected applications," *IEEE Transactions on Industry Applications*, vol. 55, no. 2, pp. 1853–1862, 2019, https://doi.org/10.1109/TIA.2018.2873534.

[40] S. Heroual, B. Belabbas, Y. Diab, M. M. Mahmoud, T. Allaoui, and N. Benabdallah, "Optimizing power flow in photovoltaic-hybrid energy storage systems: A PSO and DPSO approach for PI controller tuning," *International Transactions on Electrical Energy Systems*, vol. 2025, no. 1, p. 9958218, 2025, https://doi.org/10.1155/etep/9958218.

[41] S. Augustine, M. K. Mishra, and N. Lakshminarasamma, "A unified control scheme for a standalone solar-PV low voltage DC microgrid system with HESS," *IEEE Journal of Emerging and Selected Topics in Power Electronics*, vol. 8, no. 2, pp. 1351–1360, 2020, https://doi.org/10.1109/JESTPE.2019.2916421.

[42] M. Khalid, "A review on the selected applications of battery-supercapacitor hybrid energy storage systems for microgrids," *Energies*, vol. 12, no. 23, p. 4559, 2019, https://doi.org/10.3390/en12234559.

[43] S. Liu, X. Xie, and L. Yang, "Analysis, modeling and implementation of a switching bi-directional buck-boost converter based on electric vehicle hybrid energy storage for V2G system," *IEEE Access*, vol. 8, pp. 65868–65879, 2020, https://doi.org/10.1109/ACCESS.2020.2985772.

[44] B. R. Ravada and N. R. Tummuru, "Control of a supercapacitor-battery-PV based stand-alone DC-microgrid," *IEEE Transactions on Energy Conversion*, vol. 35, no. 3, pp. 1268–1277, 2020, https://doi.org/10.1109/TEC.2020.2982425.

[45] H. Guentri, T. Allaoui, M. Mekki, and M. Denai, "Power management and control of a photovoltaic system with hybrid battery-supercapacitor energy storage based on heuristics methods," *Journal of Energy Storage*, vol. 39, p. 102578, 2021, https://doi.org/10.1016/j.est.2021.102578.

[46] A. U. Rahman, I. Ahmad, and A. S. Malik, "Variable structure-based control of fuel cell-supercapacitor-battery based hybrid electric vehicle," *Journal of Energy Storage*, vol. 29, p. 101365, 2020, https://doi.org/10.1016/j.est.2020.101365.

[47] L. G. B. Putra, F. Wahab, and T. A. Tamba, "Design and implementation of linear quadratic regulator control for two-wheeled self-balancing robot," *Bulletin of Electrical Engineering and Informatics*, vol. 14, no. 2, pp. 931–939, 2025, https://doi.org/10.11591/eei.v14i2.8689.

[48] L. B. Lau, N. S. Ahmad, and P. Goh, "Self-balancing robot: Modeling and comparative analysis between PID and linear quadratic regulator," *International Journal of Reconfigurable and Embedded Systems*, vol. 12, no. 3, pp. 351–359, 2023, https://doi.org/10.11591/ijres.v12.i3.pp351-359.

[49] C. O. Omeje, A. O. Salau, and C. U. Eya, "Dynamics analysis of permanent magnet synchronous motor speed control with enhanced state feedback controller using a linear quadratic regulator," *Heliyon*, vol. 10, no. 4, p. e26018, 2024, https://doi.org/10.1016/j.heliyon.2024.e26018.

[50] N. Yang, J. Tang, Y. Li, G. Shi, and L. Shi, "Log-barrier search for structural linear quadratic regulators," *IEEE Transactions on Automatic Control*, vol. 70, no. 3, pp. 1965–1972, 2025, https://doi.org/10.1109/TAC.2024.3482097.

[51] N. F. Ibrahim, I. M. Elzein, M. M. Mahmoud, A. M. El-Rifaie, H. S. Hussein, and M. A. E. Eid, "Enhanced control of single-stage PV-STATCOM using hybrid MPPT and adaptive AHLMS for power quality improvement," *IEEE Access*, vol. 13, pp. 200253–200270, 2025, https://doi.org/10.1109/ACCESS.2025.3635707.

[52] M. Tarek and M. I. M. Elzein, "Sustainable energy management in islanded microgrids via HHO-BE tuned adaptive controllers and demand-side flexibility," *Engineering Reports*, vol. 8, no. 1, pp. 1–20, 2026, https://doi.org/10.1002/eng2.70561.

[53] Y. Liu, T. Qie, X. Zhang, H. Wang, Z. Wei, H. H. C. Iu, and T. Fernando, "A novel online learning-based linear quadratic regulator for vanadium redox flow battery in DC microgrids," *Journal of Power Sources*, vol. 587, p. 233672, 2023, https://doi.org/10.1016/j.jpowsour.2023.233672.

[54] A. Mukhatov, N. G. M. Thao, and T. D. Do, "Linear quadratic regulator and fuzzy control for grid-connected photovoltaic systems," *Energies*, vol. 15, no. 4, p. 1286, 2022, https://doi.org/10.3390/en15041286.

[55] F. Menzri, T. Boutabba, I. Benlaloui, L. Chrifi-Alaoui, A. Alkuhayli, U. Khaled, and M. M. Mahmoud, "Applications of novel combined controllers for optimizing grid-connected hybrid renewable energy systems," *Sustainability*, vol. 16, no. 16, p. 6825, 2024, https://doi.org/10.3390/su16166825.

[56] A. M. Ewias, S. H. Hakmi, T. H. Mohamed, M. M. Mahmoud, A. Eid, A. Y. Abdelaziz, and Y. A. Dahab, "Advanced load frequency control of microgrid using a bat algorithm supported by a balloon effect identifier in the presence of photovoltaic power source," *PLOS ONE*, vol. 18, no. 10, p. e0293246, 2023, https://doi.org/10.1371/journal.pone.0293246.

[57] C. Possieri and M. Sassano, "Solving the linear quadratic regulator problem in the policy space: The policy algebraic Riccati equation," *Automatica*, vol. 185, p. 112738, 2026, https://doi.org/10.1016/j.automatica.2025.112738.

[58] M. N. A. Hamid, F. A. Banakhr, T. H. Mohamed, S. M. Ali, M. M. Mahmoud, M. I. Mosaad, A. A. H. Albla, and M. M. Hussein, "Adaptive frequency control of an isolated microgrids implementing different recent optimization techniques," *International Journal of Robotics and Control Systems*, vol. 4, no. 3, pp. 1000–1012, 2024, https://doi.org/10.31763/ijrcs.v4i3.1432.

[59] Z. Jing, L. Gao, C. Wu, and D. Liang, "Linear quadratic regulator-based coordinated voltage and power control for flexible distribution networks," *Energies*, vol. 18, no. 2, p. 361, 2025, https://doi.org/10.3390/en18020361.

[60] H. M. I. Saleeb, M. M. Mahmoud, N. F. Ibrahim, A. Alkuhayli, U. Khaled, A. Beroual, and R. Kassem, "Highly efficient isolated multiport bidirectional DC/DC converter for PV applications," *IEEE Access*, vol. 12, pp. 114480–114494, 2024, https://doi.org/10.1109/ACCESS.2024.3442711.

[61] J. F. Patarroyo-Montenegro, F. Andrade, J. M. Guerrero, and J. C. Vasquez, "A linear quadratic regulator with optimal reference tracking for three-phase inverter-based islanded microgrids," *IEEE Transactions on Power Electronics*, vol. 36, no. 6, pp. 7112–7122, 2021, https://doi.org/10.1109/TPEL.2020.3036594.

[62] A. Fatah, T. Boutabba, I. Benlaloui, S. Drid, M. M. Mahmoud, M. M. Hussein, W. F. Mbasso, H. S. Hussein, and A. M. Ewias, "Design, and dynamic evaluation of a novel photovoltaic pumping system emulation with DS1104 hardware setup: Towards innovative in green energy systems," *PLOS ONE*, vol. 19, no. 10, p. e0308212, 2024, https://doi.org/10.1371/journal.pone.0308212.

[63] B. T. Gul, A. Rehman, H. I. Sherazi, A. Alburidy, A. Alsafrani, and O. Alrumayh, "Optimal control strategy for electric vehicle powered by PV arrays and battery using sliding mode control and linear quadratic regulator," *Scientific Reports*, vol. 15, no. 1, p. 45044, 2025, https://doi.org/10.1038/s41598-025-30545-w.